Polymer Chemistry

Accepted Manuscript

ROYAL SOCIETY OF CHEMISTRY

www.rsc.org/polymers

Polymer Chemistry

ARTICLE

Extremely uniform dispersion of MWCNTs in olefin block copolymer significantly enhances electrical and mechanical performance †

Received 00th January 20xx,
Accepted 00th January 20xx

DOI: 10.1039/x0xx00000x

www.rsc.org/

Ting Li, Jun-Hong Pu, Li-Feng Ma, Rui-Ying Bao, Guo-Qiang Qi, Wei Yang,* Bang-Hu Xie and Ming-Bo Yang

Ethylene-α-octene copolymers with different chain architectures (ethylene-α-octene random copolymer (ORC) and ethylene-α-octene block copolymer (OBC)) were adopted to prepare elastomeric composites with multi-walled carbon nanotubes (MWCNTs) through melt mixing. Extremely uniform dispersion of MWCNTs in OBC and serious aggregations of MWCNTs in ORC were observed. The percolation threshold of OBC composites was 2.5 vol. %, much lower than that of ORC composites. Rheological measurements and thermodynamic analysis revealed that the uniform dispersion of MWCNTs in OBC is due to the selectively localization of the nanotubes in molten state, and the stronger volume exclusion effect of OBC crystals in nanoscopic dimensions towards nanotubes also accounts for the developed MWCNT network after crystallization. Although OBC itself showed lower stress at a certain stretching and tensile modulus than that of ORC, the reinforcement in stress at a certain stretching and tensile modulus of OBC composites were almost twice as much as that of ORC composites at the same content of MWCNTs. Elongations of OBC composites were all higher than 1600% (even when MWCNT content is as high as 7.84 vol. %) and were always at least 200% larger than that of ORC composites at the same content of MWCNTs. The results provide significant guidance for the preparation of conductive elastomeric materials with both excellent electrical performance and mechanical properties by utilizing thermoplastic polyolefin copolymers with blocky chain architectures.

Introduction

Conductive polymer elastomers are capable of elastic stretching and substantial bending compared with conventional rigid conductive polymer composites, thereby holding great potentials for stretchable electronics, sensors, actuators, which meets the increasing need for multi-functional conductive polymer composites.1-3 One of the most efficient strategies in fabrication of conductive elastomeric materials is integrating elastomeric polymer matrix with carbon-based fillers (such as carbon nanotubes (CNTs) with excellent conductivity and mechanical behaviors). Adequate dispersion of CNTs in polymer matrix has to be guaranteed to achieve effective reinforcement in electrical performance and mechanical properties of polymer composites.4,5 Mixing methods (e.g. ultrasonic treatment, high speed shearing, coagulation method, etc.), functionalization of CNTs (e.g. purification, chemical functionalization, activation treatments, etc.), modification of polymer matrix (e.g. using conjugated polymers, etc.), utilization of a third component (e.g. surfactant, compatibilizer, etc.), and other means (e.g. in situ polymerization, mixing with polymer latex, etc.) have been utilized to improve the dispersion of CNTs.6,7 However, the dispersion of MWCNTs in conductive polyolefin elastomers with different chain architectures and the resulted comprehensive performances have not been reported yet.

Ethylene-α-olefin random copolymers (ORCs, as shown in Fig. 1a) is considered as one of the most widely used elastomeric polymers.8 Due to the broad-ranging and adjustable molar mass9 and narrower molar mass distribution10,11, ORCs synthesized by Metallocene catalysts have attracted a great interest in the past decades. However, since the melting temperature of such ORCs decreases due to the introduction of comonomers12, their applications at high temperatures are somewhat limited. Recently, a novel class of ethylene-α-olefin copolymers was produced using an innovative chain shuttling technology named as olefin block copolymers (OBCs, as shown in Fig. 1b).13-16 In chain shuttling technology, an ingenious use of chain shuttling agent to transfer growing polymer chains from one active catalyst site to another was adopted.17,18 Thus, block copolymers from a common monomer environment can be prepared. The efficient chain shuttling produces a linear multiblock copolymer that features alternating hard blocks (consisting essentially of crystalline ethylene homopolymer with very low levels of comonomer) and soft blocks (amorphous

College of Polymer Science and Engineering, Sichuan University, State Key Laboratory of Polymer Materials Engineering, Chengdu, 610065 Sichuan, China. Email: weiyang@scu.edu.cn

† Electronic Supplementary Information (ESI) available: [details of any supplementary information available should be included here]. See DOI: 10.1039/x0xx00000x

ethylene-α-olefin segment with high levels of comonomer), in which the hard and soft features are based on stiffness or crystallinity at room temperature.19 Owing to the blocky architecture and relatively higher melting point (up to 125 ºC) of the hard blocks, the olefin block copolymers exhibit excellent elastomeric properties, heat resistance and high thermal stability. Moreover, ethylene-α-olefin block copolymers are more eco-friendly to environment comparing frequently-used styrenic block copolymers, which allows them to be the most promising alternatives in thermoplastic elastomeric polymers. Hence, OBC is considered as a favorable matrix to conduct fundamental researches20 and prepare a variety of multi-functional materials.21,22

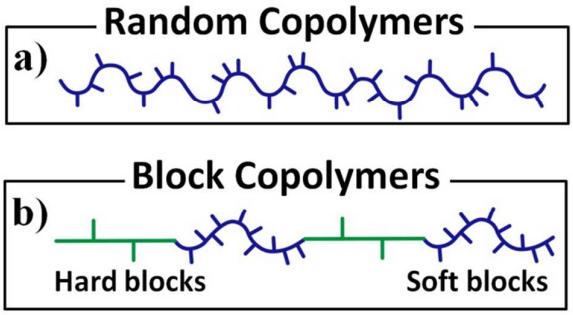

Fig. 1 Sketch showing the architectures of copolymers and the relative terminologies (a) ethylene-α-olefin random copolymer, (b) ethylene-α-olefin block copolymer.19, 23

Thus, with the purpose of enhancing electrical and mechanical performance of conductive polymer elastomer, uniform dispersion of MWCNTs by selecting appropriate chain architectures of the thermoplastic polyolefin elastomers with similar overall chemical constitution is deserved to be investigated. In this study, ethylene-α-octene copolymer with the same kind and similar content of comonomers but random or blocky architecture were adopted. Rheological measurements and thermodynamic analysis were carried out to illustrate the different dispersion of MWCNTs in molten state, Differential scanning calorimetry (DSC) and wide-angle x-ray diffraction (WAXD) revealed the distinct crystal dimensions in the OBC and ORC composites, mirroring the disparate volume exclusion effect of the crystals in copolymer-based materials towards MWCNTs in solid state. These results explain the differences of the dispersion of MWCNTs in the thermoplastic polyolefin elastomers with random and blocky architectures. As a consequence of the different dispersion, OBC elastomeric materials possess improved electrical and mechanical performances. This research is hopefully to provide a guidance for the preparation of conductive thermoplastic polyolefin elastomeric materials with improved comprehensive performances.

Experimental section

Materials

Ethylene-octene copolymers with different molecular architectures were from Dow Chemical Co. (Midland, MI, USA). The octene units in ORC (Engage 8150) are randomly distributed along the whole polymer chain, with an octene content of 39 %.24 OBC (Infuse 9500)was synthesized by chain shuttling polymerization technology, consisting of nearly amorphous soft blocks and crystallizable hard blocks, with a total octene content of 38 %, namely, the same kind of comonomer and similar octene content as ORC (For more details, see Table S1†). MWCNTs (XFM13), with an average diameter of 10-20 nm and length of 10-30 μm, were purchased from XFNANO Inc. (Nanjing, China) and used as-received without further treatment. The density of MWCNT is 1.8 g/cm^3.25,26

Sample preparation

Elastomeric materials consisting of MWCNTs and copolymers were prepared by melt mixing in an internal mixer (XSS-300, Shanghai Kechuang Rubber Plastics Machinery Set Ltd, China) at 50 rpm and 150 ºC. These two series of composites were both melt compounded in two steps to optimize the dispersion of MWCNTs. First, copolymers and MWCNTs were melt compounded for 5 min to prepare a MWCNT/polymer master batch with a certain content of MWCNTs; then the master batch was pulverized with a high-speed mechanical pulverizer at a speed of 25 000 rpm for 3 min to improve the dispersion, and the pulverized master batch was diluted with raw resins to set contents of MWCNTs in the same internal mixer under the same conditions for another 5 min.

The resulted samples were marked as ORC-x and OBC-x, where ORC and OBC represent the elastomeric materials based on the former or the latter with MWCNTs, respectively, and x stands for the volume fraction of nanotubes in the composites. After compounding, all the composites were compression molded into sheets with a thickness of about 1.2 mm at 150 ºC for 10 min under a pressure of 10 MPa.

Characterization

Dispersion of MWCNTs

The dispersion of MWCNTs in the conductive elastomeric materials was characterized with a JEOL JSM-5900LV scanning electron microscope (SEM, Japan)27 at an accelerating voltage of 20 kV. The compression molded composites were immersed in liquid nitrogen for 45 min, and then quickly impact fractured. All the fresh surfaces were sputter coated with gold prior to examination.

Furthermore, the dispersion states of MWCNTs at the microcosmic scale were observed with a transmission electron microscopy (TEM, Philips CM120)28-30 equipped with a field emission gun (FEG) at 200 kV. Ultrathin sample sections with a thickness of 50-100 nm were cut on a Leica EM UC6 ultra-microtome (Leica Microsystems, Wetzlar, Germany)31 at -120 ºC.

Electrical conductivity

For the characterization of room-temperature volume resistivity, the compression molded composites were cut into rectangular sheets with a dimension of 1.2 mm × 10 mm × 30 mm (both sides of the

samples were coated with silver paste to reduce the contact resistance) and 1.2 mm × 150 mm × 150 mm, respectively. Then the volume resistivity of the samples were measured consecutively by employing a digital multimeter (6517B, Keithley Instruments, Inc, Ohio, USA) (below 10^6 Ω) and a high-resistivity meter (ZC36, Shanghai Precision Instruments Co., Ltd. China) (above 10^6 Ω), respectively. At least ten samples were tested for each measurement and the average results were provided. Before characterization, all the samples were stored at room temperature for one week.

Rheological tests

Rheological measurements were carried out on a stress-controlled rotational rheometer (AR2000EX, TA instruments, USA) in a dynamic frequency sweep from 0.01 to 100 Hz at a strain of 1% within the linear viscoelastic region at 150 °C. The samples were prepared by thermally compressing the composites into plates with a thickness of 1.2 mm and diameter of 25 mm at 150 ºC for 10 min under 10 MPa.

Differential scanning calorimetry (DSC)

The melting behaviors of the composites were measured using a differential scanning calorimeter (DSC, TA Q20, USA). 3-5 mg samples were cut from compression-molded sheets for thermal analysis. The samples were firstly heated up to 150 ºC at a rate of 10 ºC min^{-1} under a nitrogen atmosphere and held at 150 ºC for 2 min to eliminate the thermal history. After that, the samples were cooled to 10º C at a rate of 10 ºC min^{-1} to record the crystallization behavior, and then heated again to 150ºC at a rate of 10 ºC min^{-1} to record the melting behavior. The temperature was calibrated with indium. The crystallinity of the samples is estimated based on the ratio of the measured melting enthalpies to that of perfect PE crystals (ΔHm, PE = 290 J/g). ,

Wide-angle X ray diffraction (WAXD)

Wide-angle X-ray diffraction (WAXD) patterns of the samples were obtained using a DX-1000 diffractometer with Cu Kα radiation (λ = 0.154 nm) at a voltage of 40 kV and a current of 40 mA. Samples were scanned over the range of diffraction angle 2θ = 2-35º, with a speed of 3º min^{-1} at room temperature.

Mechanical properties

The mechanical performances testing was performed on an AGS-J universal material testing machine (the maximum capacity of the load cell was limited to 10 kN) at room temperature with a gauge length of 10 mm. All the samples used for mechanical performance testing were dumb-bell32 ones with a dimension of 10 mm × 2 mm × 1.2 mm. The uniaxial tensile fracture test was carried out at a crosshead speed of 100 mm/min. At least five samples were tested repeatedly and the average results were reported. Before characterization, all the samples were stored at room temperature for one week.

Results and discussion

Dispersion of MWCNTs

The dispersion states of MWCNTs in the two series of conductive elastomeric materials were examined by SEM. The images of the conductive elastomeric materials with relatively low (2.48 vol. %) and high (7.84 vol. %) content of MWCNT are shown in Fig. 2. The ORC composites hold a disordered network with MWCNT cluster rich and sparse regions, as indicated by the light circles in Fig. 2a and c. The aggregation of MWCNTs is more obviously when their content is relatively low, corresponding to a poor distribution in ORC composites. In stark contrast, OBC composites distribute uniformly and pack densely with MWCNT, even in the amplificatory images shown in the inserts of Fig. 2b and d.

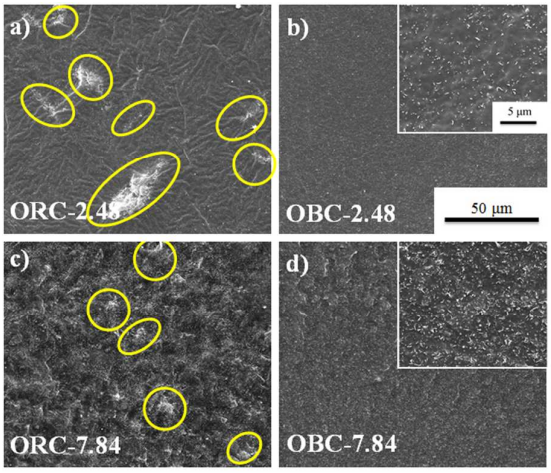

Fig. 2 SEM images of (a) ORC-2.48, (b) OBC-2.48, (c) ORC-7.84, and (d) OBC-7.84.The light circles in (a) and (c) indicate the aggregated MWCNT bundles, and the inserts in (b) and (d) are local amplifications.

TEM observation was carried out to reveal the dispersion of MWCNTs visually at a more microcosmic scale. Fig. 3 shows the TEM images of ORC- and OBC-2.48 and the dark lines represent MWCNTs distributed in the matrix. As shown in Fig. 3a, MWCNTs in ORC-2.48 are not so well dispersed and serious aggregations of MWCNTs are visible in the whole scope, especially in the zoom-in image shown in Fig. 3c. However, well-dispersed MWCNTs are observed for OBC-2.48 as shown in Fig. 3b and d. It's worth noting that the dispersion of MWCNTs is so uniform that a lot of single MWCNTs are visible as indicated in Fig. 3d. These results agree well with the SEM observation, and the reason for the uniform dispersion of MWCNTs in OBC composites will be analyzed in detail in the following section.

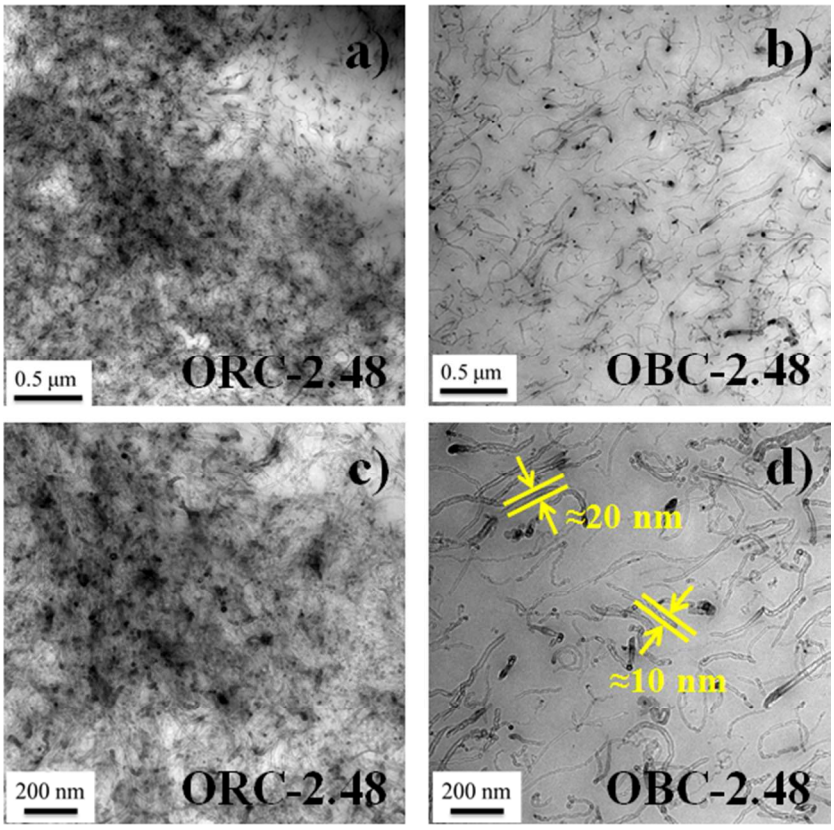

Fig. 3 Typical TEM images of (a) ORC-2.48, (b) OBC-2.48, (c) and (d) are the local amplifications of (a) and (b), respectively.

Electrical properties

Fig. 4a depicts the conductivity (σ) as a function of overall MWCNTs volume fraction in the conductive elastomeric composites. The conductivity for both ORC and OBC conductive composites increases with increasing MWCNTs content. The sudden change in the conductivity of conductive composites around a certain content is generally described by a scaling law according to classical percolation theory33-35 shown in Equation (1),

$$\sigma = \sigma_0(\phi - \phi_c)^t \quad (1)$$

where σ_0 is a scaling factor, σ is the electrical conductivity of conductive composites, t is the critical exponent revealing the dimensionality of the conductive networks, ϕ is the volume content of MWCNTs, and ϕ_c is the threshold of the electrical conductivity percolation.

The electrical conductivity percolation threshold, ϕ_c, of conductive composites can be determined through fitting of classical percolation theory to experimentally obtained conductivity,36-38 as shown in Fig. 4b. The percolation threshold of OBC composites is observed to be 2.5 vol. %, much lower than that of ORC composites, 9 vol. %, as reported in our previous work39 and other researches.40 Because of the same kind and similar content of comonomers in ORC and OBC, as well as the same preparation procedure of the composites, the results clearly show a predominant contribution of chain architectures of the polymer matrix to the electrical properties of the composites. Obviously, OBC is more appropriate to prepare conductive elastomeric materials with relatively lower content of MWCNTs.

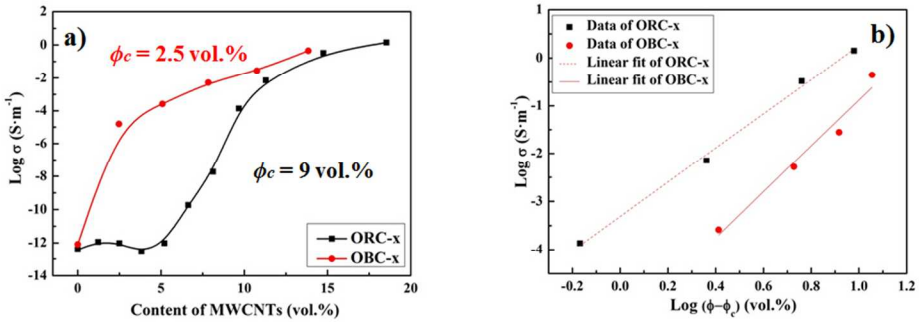

Fig. 4 (a) Log σ as a function of MWCNTs content; (b) A log-log plot of conductivity versus ϕ - ϕ_c and the fitting of experimental results with percolation law. Here, the electrical performance of ORC composites were the same with our previous report.39

According to Li et al.41, the critical factors. Including the aspect ratio of CNTs, disentanglement of CNT agglomerates, and the uniform dispersion of individual CNTs or CNT agglomerates, determine the percolation threshold of polymer/CNT nanocomposites. The distinctly different percolation thresholds of these two series of elastomeric composites with exactly the same kind of carbon nanotube, therefore, are principally from the dispersion state of MWCNTs in the matrix. With all other conditions maintaining invariant, the higher electrical conductivity at lower conductive filler content stems from a more developed conductive pathways primarily due to the uniform dispersion of MWCNT.

Analysis of the molten state

Rheological measurements were utilized widely to analyze the MWCNT network in polymer/carbon filler systems, 42-44 To reveal the existence and microstructure of MWCNT network in both series of elastomeric composites, dynamic rheological behaviors were measured at 150 ºC as a function of frequency and the results are shown in Fig. 5. It can be observed that pure ORC and OBC show only very slight difference of storage modulus (G') and loss tangent (tan δ, defined as ratio between the loss modulus (G'') and G'), indicating that the significantly varied rheological properties of the composites can be mainly attributed to the introduction and the distinctly different dispersion state of MWCNTs.

With the increasing loading of MWCNTs, nanotube-nanotube interactions begin to dominate, and eventually lead to the percolation and formation of an interconnected structure. Thus, the storage modulus of the conductive elastomeric materials increase as shown in Fig. 5a. Meanwhile, large-scale polymer relaxations in the composites are effectively restrained by the presence of MWCNTs, thus the low frequency power-law dependence of G' decreases monotonically. When the loading of MWCNTs is relatively high (7.48 vol. %), the storage modulus of both series of composites are almost independent of the frequency at low frequencies, indicative of a transition from liquid-like to solid-like viscoelastic behavior. This nonterminal low frequency behavior can be attributed to the formed MWCNT network, which restrains the long-range motion of polymer chains significantly.

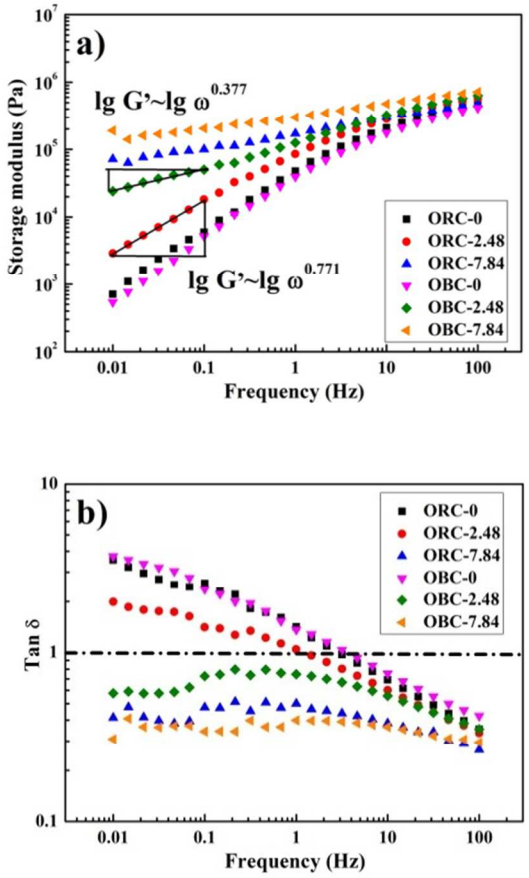

Fig. 5 (a) Logarithmic plots of storage modulus as a function of frequency and (b) logarithmic plots of loss tangent (tan δ) vs. frequency.

It can be seen that the storage modulus of OBC composites is always higher than that of ORC composites at the same content of MWCNTs and the same frequency. The storage modulus plateau at low frequency are more evident in OBC composites. The slopes derived in the low-frequency terminal region of lg G'-lg ω curve of OBC-2.48 is 0.377, much lower than that of ORC-2.48 (0.771). These results clearly show a more effective restraint of large-scale

polymer relaxations in OBC composites, indicating the network of nanotubes is better developed due to the better dispersion of MWCNTs in OBC composites.

Fig. 5b gives the relationship between the loss tangent (tanδ) for both series of composites with different MWCNT loadings with respect to the oscillatory frequency. Tan δ is often used to characterize the viscoelasticity of a material and a lower value of tanδ means that the material performs relatively more solid-like. Compared with pure ORC or OBC, the elastomeric composites with MWCNT exhibit a lower tanδ. At the same MWCNT concentration, tanδ of OBC composites is always lower than that of ORC composites. Especially, the tanδ of OBC-2.48 is lower than 1, while that of ORC-2.48 is higher than 1, suggesting a more densely packed MWCNT network in OBC composites. Therefore, these results also suggest that the MWCNT network of OBC composites is better developed with lower nanotube content due to a more uniform dispersion, which also contributes to the lower percolation threshold.

The above mentioned results agree well with the SEM and TEM examination as can be seen in Fig. 2 and Fig. 3 as well as the percolation behavior shown in Fig. 4, where much lower percolation threshold have been achieved in OBC composites.

According to Al-Saleh et al.,45 selective localization of conductive filler at the interface of immiscible polymer blends can be realized by introducing block copolymer. They reported that styrene-butadiene-styrene block copolymer (SBS) is localized at the interface between polypropylene (PP) and polystyrene (PS), meanwhile, carbon black (CB) shows higher affinity to polybutadiene (PBD) segments in SBS as analyzed by classical thermodynamics, thus CB can selectively localize in SBS, which is right at the interface between PP and PS. Hence, in this work, the uniform dispersion of MWCNTs in OBC matrix may be closely related with the affinity of MWCNTs to the different domains of the elastomeric materials in the molten state.

Moreover, considering that the rheological behaviors are all obtained in the molten states, the affinity between MWCNTs and rich domains formed by chain sequences is likely to be the main reason for the different dispersion state of MWCNTs. Classical thermodynamics, therefore, were utilized here to calculate the affinity of MWCNTs to different domains of the elastomeric materials in the molten state.

As is known, ORC consists of random ethylene-α-octene copolymer, but the hard blocks of OBC mainly consisted of crystalline long polyethylene (PE)-like sequences and the soft blocks are composed of random ethylene-α-octene copolymer.19 Thus, ORC can be regard as a material with completely ethylene-α-octene rich domains while OBC is considered to be the combination of polyethylene-rich domains and ethylene-α-octene-rich domains in the molten state. Moreover, the surface energy (γ) of the polyethylene-rich domains and ethylene-α-octene-rich domains can be described by γ of polyethylene and ethylene-octene copolymer, respectively. It is worth mentioning that the use of surface energies of ORCs in previous researches is relatively arbitrary without considering the octene content as discussed in Table S2†. Therefore, we think it is reasonable to use the surface energies of ORC with 39 wt.% octene content to describe the ethylene-α-octene-rich domains of ORC and OBC during our calculation. The higher interfacial energy of the filler towards a certain component implies the lower affinity between them. The interfacial energies were calculated from the surface energies of the dispersion and polar parts. The harmonic and the geometric mean equation are two main approaches according to the type of surfaces.46 Here, both of the equations are applied as follows,

Harmonic mean equation:

$$\gamma_{12} = \gamma_1 + \gamma_2 - 4\left[\frac{\gamma_1^d\gamma_2^d}{\gamma_1^d + \gamma_2^d} + \frac{\gamma_1^p\gamma_2^p}{\gamma_1^p + \gamma_2^p}\right] \quad (2)$$

Geometric mean equation:

$$\gamma_{12} = \gamma_1 + \gamma_2 - 2\left(\sqrt{\gamma_1^d\gamma_2^d} + \sqrt{\gamma_1^p\gamma_2^p}\right) \quad (3)$$

where γ_1 and γ_2 are the surface energies of components 1 and 2; γ_1^d and γ_2^d are the dispersive parts of the surface energies of components 1 and 2; γ_1^p and γ_2^p are the polar parts of the surface energies of components 1 and 2.47-49

The surface free energies of the materials at 190 ºC (higher than T_m of ORC or OBC) were used. The values of the surface free energies, as well as the dispersion and polar components of MWCNT, polyethylene-rich and ethylene-α-octene-rich domains were listed in Table 1.

Table 1. Surface free energies of MWCNT, polyethylene-rich and ethylene-α-octene-rich domains at 190 ºC, respectively.

Materials	Total surface energy γ (mJ m^{-2})	Dispersion component γ^d (mJ m^{-2})	Polar component γ^p (mJ m^{-2})
MWCNT[a]	45.3	18.4	26.9
MWCNT[b]	27.8	17.6	10.2
ethylene-α-octene-rich domains [c]	17.5	15.6	1.9
polyethylene-rich domains [d]	25.9	25.9	0

a. According to Nuriel et al.50 and Zeng et al.51.
b. According to Barber et al.52 and Baudouin et al.53.
c. described with that of ethylene-olefin random copolymer54.
d. described with that of polyethylene55.

According to the values in Table 1, the interfacial energies between MWCNT, polyethylene-rich and ethylene-α-octene-rich domains using the harmonic and geometric mean equation were calculated and summarized in Table 2. It can be seen that the MWCNTs show lower affinity to polyethylene-rich domains, as revealed by the higher interfacial energy calculated by both equations. Hence, after melt mixing, the broken MWCNT bundles

(broken by shear stress during melt mixing) selectively localized in OBC composites in the molten state due to this weak binding, and resulted in a promoted MWCNT dispersion in OBC elastomeric composites. Meanwhile, MWCNTs did not show a selective localization in ORC-based materials since there is only ethylene-α-octene domains.

Table 2. Interfacial energies calculated using harmonic and geometric mean equations.

Materials	By harmonic mean equation (mJ m^{-2})	By geometric mean equation (mJ m^{-2})
MWCNT[a]/ ethylene-α-octene-rich domains	21.9	14.6
MWCNT[a]/ polyethylene-rich domains	28.2	27.5
MWCNT[b]/ ethylene-α-octene-rich domains	5.8	3.4
MWCNT[b]/ polyethylene-rich domains	11.8	11.0

a. according to Nuriel et al.50 and Zeng et al. 51.

b. according to Barber et al. 52 and Baudouin et al. 53.

In addition, those results indicated by rheological measurements and thermodynamic analysis are also in good accordance with the conclusions drawn by Banerjee et al.56 and Feng et al.57 using molecular dynamics simulation. that is, larger particles (sufficiently larger than the monomer diameter) in copolymers provide better dispersion than both homopolymers and random copolymers, and the preferential localization of conductive nanoparticles in a continuous block of diblock copolymers can dramatically reduce the percolation threshold.

Analysis of the solid state after crystallization

Previous researches58-61 reported that the higher electrical conductivity with lower conductive filler content stems from the presence of more developed conductive pathways. These pathways can be due to the crystallization driven exclusion of the conductive fillers into the inter-crystal region, known as the volume exclusion effect. In the views of Hölzer et al.62 and Zuo et al.12 , the hard blocks in OBC are long enough without many branches to fold back and forth into larger folded lamellar crystals with nanoscopic dimensions. Comparing the long PE-like sequences in OBC, the high comonomer content in ORC leads to poor crystallizability and much smaller fringed micelles or bundles crystals. Thus, as a result of distinct crystal dimensions, different volume exclusion effect of OBC and ORC crystals to MWCNTs can account for the dispersion of nanotubes and the development of MWCNT network.

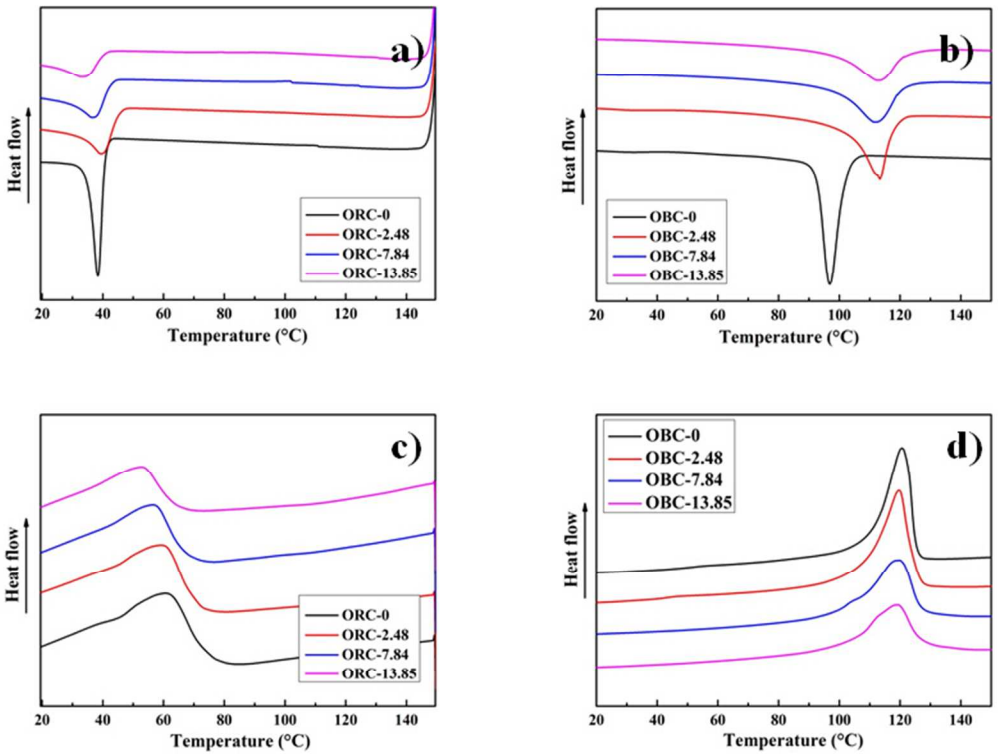

Fig.6 (a) and (b) Cooling curves obtained after the first heating, (c) and (d) melting curves for ORC and OBC elastomers, respectively. The curves are vertically shifted for easier visualization.

Table 3. Parameters from DSC melting and cooling scans for the conductive elastomers. Xc are normalized for clarity.

	ORC composites				OBC composites			
	0	2.48	7.84	13.85	0	2.48	7.84	13.85
Tc (ºC)	38.47	40.12	37.63	34.57	101.87	113.35	111.41	112.45
Hc (J/g)	14.20	12.60	11.39	9.97	44.06	44.69	39.76	38.39
Tm (ºC)	61.83	60.37	57.28	53.09	120.57	119.57	119.01	118.44
Hm (J/g)	14.30	13.44	12.66	12.03	53.59	55.66	47.00	45.03
Xc (%)	4.93	4.64	4.37	4.15	18.48	19.19	16.21	15.53

To clarify the larger crystals in OBC comparing that in ORC as mentioned above, DSC and WAXD were conducted.

As can be seen in Fig.6a and b, the crystallization temperatures, Tcs, of OBC composites are always higher than those of ORC composites irrespective of the existence of MWCNTs, showing the better crystallization capacity of OBC composites due to the long crystallizable hard blocks. As a consequence, OBC composites can develop more perfect crystals. Interestingly, all the Tcs of OBC composites shift to higher temperature compared with ORC composites after the addition of MWCNTs, implying a better heterogeneous nucleation effect of nanotubes for OBC. These results can be interpreted from the more uniform dispersion of MWCNTs in OBC composites as discussed above.

In addition, the first heating scans of ORC and OBC composites are shown in Fig.6c and d. Parameters from the scans were collected in Table 3. The OBC composites exhibit significantly higher melting points than that of ORC elastomers. The melting points of OBC based materials are only 5~10 ºC lower than the melting temperatures of the classical, orthorhombic PE crystals, suggesting much better heat resistance of OBC composites when compared with ORC composites. The narrower melting temperature range of OBC composites demonstrates their perfect crystalline structures. The melting enthalpies of ORC elastomers are only 12~14 J/g, which corresponds to an very low overall crystallinity of Xc = 4.1 ~ 4.9% based on the melting enthalpy of perfect PE crystals (ΔHm,PE=290 J/g), owing to the destroyed regularity and symmetry of chain architecture in ORC. On the contrary, the melting enthalpies of OBC elastomers are 45~55 J/g, leading to an overall crystallinity Xc = 15.5~19.2%, due to the hard blocks and better heterogeneous nucleation effect of MWCNTs.

Moreover, with increasing MWCNT content, and the growth of crystals in both series was kinetically hindered by the geometrical constraints of nanotubes, resulting in decreased Xcs. Reduction in Xcs of OBC was more serious as a result of more uniform dispersion of MWCNTs, which hindered the growth of OBC crystal.

The Broadhurst equation63-65 was used to approximate the lamellar thickness of these conductive elastomers

$$T_m^n = T_m^\infty \frac{a+n}{b+n} \quad (4)$$

where T_m^∞= 140.15 ºC is the melting point of an ideal PE crystal with infinite lamella thickness and a=1.5 and b = 5.0 are the fitting parameters to describe the melting behavior of alkanes and PE crystals. On the basis of the relationship between melting temperature and thickness of PE lamella reported by Hölzer et al. (as shown in Fig.1 in ref. 62), here, the peak characterizing a low temperature) at 30~80 ºC for ORC composites correspond to lamella thicknesses of 2 to 4 nm. The lamella thickness of OBC composites with high melting temperature, however, are about 12 nm, indicating a much larger average dimension of the PE-like lamella in OBC composites when compared with ORC composites., which can be attributed to long PE-like hard blocks in OBC.

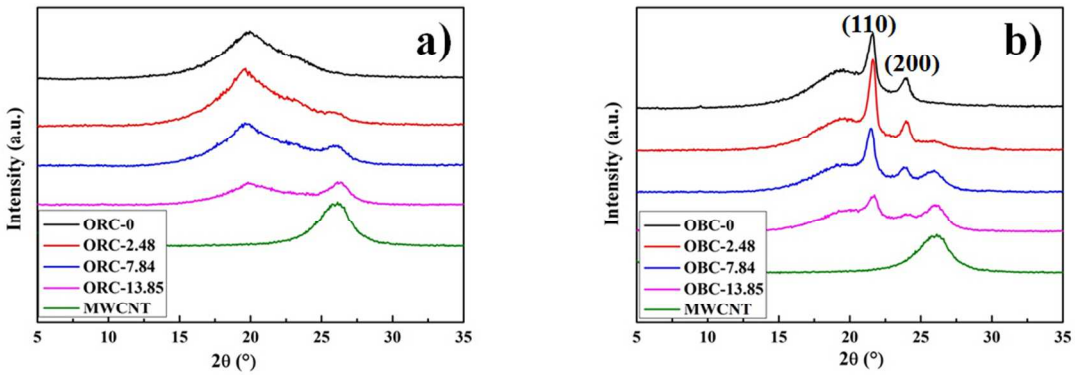

Fig.7 WAXD patterns for conductive (a) ORC and (b) OBC elastomers. The patterns are vertically shifted for clarity.

WAXD can be an ideal method to explore the crystalline structure, crystallinity and microcrystal dimension of the matrix polymers in conductive elastomers.66 As reported in ref. 67, the characteristic diffraction peaks at 21.6° and 23.9° in WAXD patterns, corresponding to interplanar spacing of 0.43 and 0.38 nm, can mirror the (110) and (200) reflections of orthorhombic PE crystals. As shown in Fig.7, the (110) and (200) reflections of ORC are too weak to see while those of OBC composites are sharp enough to identify, indicating that OBC composites has higher crystallinity, perfect crystals and larger orthorhombic microcrystals, leading to stronger volume exclusion effect.

As reported by Hölzer et al.,62 the amorphous regions between OBC crystals also have nanoscopic dimensions, thus the MWCNTs (with an average diameter of 10-20 nm) can selectively localized in nanoscopic amorphous regions due to the stronger volume exclusion effect of larger OBC crystals, and resulting in exhibition of several single MWCNTs as can be seen in Fig.3. In contrast, volume exclusion effect of ORC crystals is limited, attributed to much smaller crystals, as a consequence, MWCNTs can almost localized aggregately without enough affection.

Mechanical properties

The uniaxial stress-strain curves for all conductive elastomeric composites can characterize some of the mechanical properties of typical thermoplastic elastomers, i.e., diffused yielding point, strain-hardening at the late stage and large strain at break as depicted in Fig. S1†. Average values of the important mechanical parameters are plotted versus MWCNT contents in Fig. 8. The pure OBC shows lower stress at a certain stretching and tensile modulus than the ORC, which agrees well with the previous research from Zuo et al.12. Nevertheless, percentages of reinforcement in mechanical properties of OBC composites are almost twice as much as those of ORC composites at the same loading of MWCNT. We can, therefore, conclude that the improvements of stress at a certain stretching and tensile modulus are mainly due to the more homogeneous dispersion and well-developed network of MWCNTs in OBC composites.

In Fig. 8c, the tensile elongation at break of OBC composites is always higher than 1600% even when the content of MWCNT is high as 7.84 vol. %, and the elongation of OBC composites is at least 200% larger than that of ORC composites at the same content of MWCNTs. This is because according to previous researches,68-70 the large elongation at break of polymers mainly depends on the average length of flexible chain segments between two adjacent crystallites serving as physical cross-link junctions. The blocky molecular architecture of OBC chains results in long and flexible chain segments between crystals. These flexible chain segments can be stretched easily as reported by Wang et al.,71 leading to lower repulsive forces due to entropy elasticity and hence larger elongation compared to ORC.

As indicated above, the mechanical properties of ethylene-octene copolymer based conductive elastomeric composites can be easily tuned by the chain architectures of the copolymer. Typically, larger tensile modulus, stress, and strain at break can be achieved with a blocky architecture. Different tensile behavior of ethylene-octene copolymers can be interpreted in terms of their different dispersion state of and developed network of MWCNTs. Especially, uniform dispersion and better developed network of MWCNTs in OBC composites show a significant reinforcement effect in the nanocomposites compared with those in the ORC composites. This effect can be derived from their chain structure and further contribute to the higher stress and modulus.

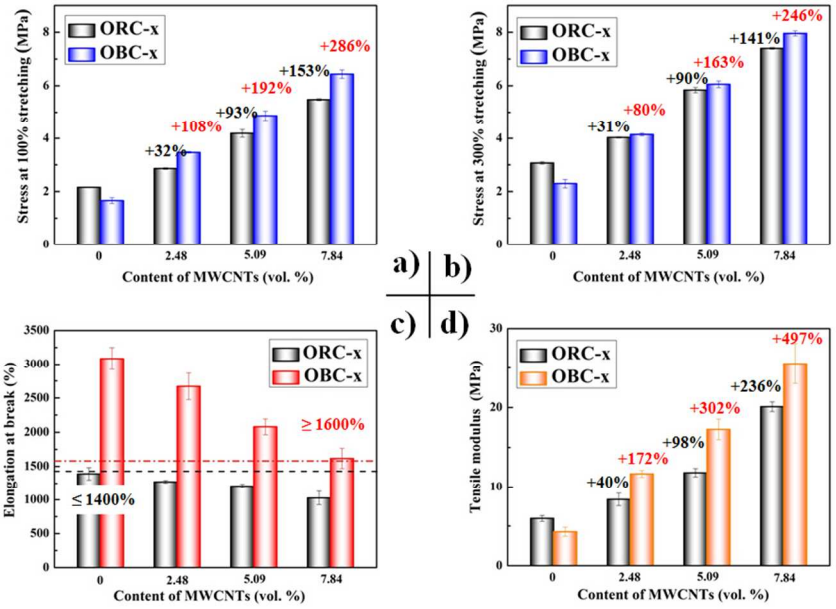

Fig. 8 (a) Stress at 100% stretching, (b) Stress at 300% stretching, (c) Elongation at break and (d) Tensile modulus of ORC composites and OBC composites. Percentages in (a), (b) and (d) are the percentages of reinforcement in stress at 100% stretching, stress at 300% stretching and tensile modulus, respectively when compared with each pure polymer matrix.

Conclusions

Ethylene-α-octene copolymer with different chain architectures were adopted to prepare elastomeric composites with MWCNTs through melt mixing. The MWCNTs dispersed uniformly in OBC composites while aggregated seriously in ORC composites. Selectively localization of MWCNTs due to the lower affinity towards the hard blocks of OBC was the main cause of the uniform dispersion of nanotubes in OBC composites in the molten state. Larger crystals and amorphous regions with nanoscopic dimensions in OBC composites lead to stronger volume exclusion effect and resultantly more developed conductive pathways comparing those in ORC composites. The percolation threshold of OBC composites is much lower than that of ORC composites due to the more homogeneous dispersion and well-developed network of MWCNTs in former composites. The percentages of reinforcement in stress at a certain stretching and tensile modulus of OBC composites are almost twice as much as those of ORC composites at the same content of MWCNTs composites. Elongation of OBC composites is all higher than 1600%, and at least 200% larger than that of ORC composites at the same content of MWCNTs. The results demonstrated that conductive thermoplastic polyolefin elastomeric composites with significantly improved electrical performance and mechanical properties can be achieved by ethylene-α-octene copolymer with appropriate chain architectures.

Acknowledgements

This work was supported by the National Natural Science Foundation of China (NNSFC Grants 51422305 and 51421061), Major State Basic Research Development Program of China (973 program) (2011CB606006), the Innovation Team Program of Science & Technology Department of Sichuan Province (Grant 2014TD0002) and Sichuan Provincial Science Fund for Distinguished Young Scholars (2015JQO003).

Notes and references

1. S. K. Yadav, I. J. Kim, H. J. Kim, J. Kim, S. M. Hong and C. M. Koo, *J. Mater. Chem. C,* 2013, **1**, 5463-5470.
2. Y. Li and H. Shimizu, *Macromolecules*, 2009, **42**, 2587-2593.
3. D. Wang, H. Li, M. Li, H. Jiang, M. Xia and Z. Zhou, *J. Mater. Chem. C*, 2013, **1**, 2744-2749.
4. P.-C. Ma, N. A. Siddiqui, G. Marom and J.-K. Kim, *Composites Part A*, 2010, **41**, 1345-1367.
5. L. Bokobza, *Polymer*, 2007, **48**, 4907-4920.
6. N. Grossiord, J. Loos, O. Regev and C. E. Koning, *Chem. Mater.*, 2006, **18**, 1089-1099.
7. X.-L. Xie, Y.-W. Mai and X.-P. Zhou, *Mater. Sci. Eng., R*, 2005, **49**, 89-112.
8. S. Bensason, J. Minick, A. Moet, S. Chum, A. Hiltner and E. Baer, *J. Polym. Sci., Part B: Polym. Phys.*, 1996, **34**, 1301-1315.
9. C. Piel, F. J. Stadler, J. Kaschta, S. Rulhoff, H. Münstedt and W. Kaminsky, *Macromol. Chem. Phys.*, 2006, **207**, 26-38.
10. R. Mülhaupt, *Macromol. Chem. Phys.*, 2003, **204**, 289-327.
11. L. L. Böhm, *Angew. Chem. Int. Ed.*, 2003, **42**, 5010-5030.
12. F. Zuo, C. Burger, X. Chen, Y. Mao, B. S. Hsiao, H. Chen, G. R. Marchand, S.-Y. Lai and D. Chiu, *Macromolecules*, 2010, **43**, 1922-1929.
13. H. Wang, D. Khariwala, W. Cheung, S. Chum, A. Hiltner and E. Baer, *Macromolecules*, 2007, **40**, 2852-2862.
14. A. Kamdar, H. Wang, D. Khariwala, A. Taha, A. Hiltner and E. Baer, *J. Polym. Sci., Part B: Polym. Phys.*, 2009, **47**, 1554-1572.
15. D. Khariwala, A. Taha, S. Chum, A. Hiltner and E. Baer, *Polymer*, 2008, **49**, 1365-1375.
16. I. W. Hamley, *The physics of block copolymers*, Oxford University Press New York, 1998.
17. V. C. Gibson, *Science*, 2006, **312**, 703-704.
18. D. J. Arriola, E. M. Carnahan, P. D. Hustad, R. L. Kuhlman and T. T. Wenzel, *Science*, 2006, **312**, 714-719.
19. H. E. Park, J. M. Dealy, G. R. Marchand, J. Wang, S. Li and R. A. Register, *Macromolecules*, 2010, **43**, 6789-6799.
20. X. Zhou, J. Feng, D. Cheng, J. Yi and L. Wang, *Polymer*, 2013, **54**, 4719-4727.
21. Q. Zhang, K. Cui, J. Feng, J. Fan, L. Li, L. Wu and Q. Huang, *Sol. Energy Mater. Sol. Cells*, 2015, **132**, 632-639.
22. Q. Zhang and J. Feng, *Sol. Energy Mater. Sol. Cells*, 2013, **117**, 259-266.
23. G. Liu, Y. Guan, T. Wen, X. Wang, X. Zhang, D. Wang, X. Li, J. Loos, H. Chen and K. Walton, *Polymer*, 2011, **52**, 5221-5230.
24. R. R. Tiwari and D. Paul, *Polymer*, 2011, **52**, 5595-5605.
25. J. Ji, G. Sui, Y. Yu, Y. Liu, Y. Lin, Z. Du, S. Ryu and X. Yang, The *J. Phys. Chem. C*, 2009, **113**, 4779-4785.
26. T. Takeda, Y. Shindo, Y. Kuronuma and F. Narita, *Polymer*, 2011, **52**, 3852-3856.
27. L.-L. Sun, Z.-G. Zhang and W.-H. Zhong, *J. Mater. Chem.*, 2011, **21**, 944-950.
28. Z. Tang, H. Kang, Q. Wei, B. Guo, L. Zhang and D. Jia, *Carbon*, 2013, **64**, 487-498.
29. S. Wu, T. Lin and B. Guo, Nanotechnology, 2013, 24, 465708.
30. L. Wang, N. Ning, L. Zhang, Y. Lu, M. Tian and T. Chan, *Composites Part A*, 2013, **47**, 135-142.
31. B. Krause, R. Boldt, L. Häußler and P. Pötschke, *Compos. Sci. Technol.*, 2015, **114**, 119-125.
32. L. L. Wang, L. Q. Zhang and M. Tian, *Mater. Des.*, 2012, **39**, 450-457.
33. Y. Tan, L. Fang, J. Xiao, Y. Song and Q. Zheng, *Polym. Chem.*, 2013, **4**, 2939-2944.
34. B. Mathieu, C. Anthony, A. Arnaud and F. Lionel, *J. Mater. Chem. C*, 2015, **3**, 5769-5774.
35. J. D. Mendez and C. Weder, *Polym. Chem.*, 2010, **1**, 1237-1244.
36. Z. Spitalsky, D. Tasis, K. Papagelis and C. Galiotis, *Prog. Polym. Sci.*, 2010, **35**, 357-401.
37. Z.-c. Shi, S.-g. Chen, R.-h. Fan, X.-a. Wang, X. Wang, Z.-d. Zhang and K. Sun, *J. Mater. Chem. C*, 2014, **2**, 6752-6757.
38. J. Zhang, M. Mine, D. Zhu and M. Matsuo, *Carbon*, 2009, **47**, 1311-1320.
39. T. Li, L.-F. Ma, R.-Y. Bao, G.-Q. Qi, W. Yang, B.-H. Xie and M.-B. Yang, *J. Mater. Chem. A*, 2015, **3**, 5482-5490.
40. P. Slobodian, P. Riha, R. Olejník, M. Kovar and P. Svoboda, *Journal of Nanomaterials*, 2013, **2013**, 5.
41. J. Li, P. C. Ma, W. S. Chow, C. K. To, B. Z. Tang and J. K. Kim, *Adv. Funct. Mater.*, 2007, **17**, 3207-3215.
42. C.-L. Huang and C. Wang, *Carbon*, 2011, **49**, 2334-2344.
43. S. Bar-Chaput and C. Carrot, *Rheol. Acta*, 2006, **45**, 339-347.
44. Q. Zhang, F. Fang, X. Zhao, Y. Li, M. Zhu and D. Chen, *J.*

Phys. Chem. B, 2008, **112**, 12606-12611.
45. M. H. Al-Saleh and U. Sundararaj, *Composites Part A*, 2008, **39**, 284-293.
46. H.-J. Butt, K. Graf and M. Kappl, *Physics and chemistry of interfaces*, John Wiley & Sons, 2006.
47. M. T. Müller, P. Pötschke and B. Voit, *Polymer*, 2015, **66**, 210-221.
48. J.-W. Zha, W.-K. Li, R.-J. Liao, J. Bai and Z.-M. Dang, *J. Mater. Chem. A*, 2013, **1**, 843-851.
49. K. Premphet and P. Horanont, *Polymer*, 2000, **41**, 9283-9290.
50. S. Nuriel, L. Liu, A. Barber and H. Wagner, *Chem. Phys. Lett.*, 2005, **404**, 263-266.
51. Y. Zeng, P. Liu, J. Du, L. Zhao, P. M. Ajayan and H.-M. Cheng, *Carbon*, 2010, **48**, 3551-3558.
52. A. H. Barber, S. R. Cohen and H. D. Wagner, *Phys. Rev. Lett.*, 2004, **92**, 186103.
53. A.-C. Baudouin, J. Devaux and C. Bailly, *Polymer*, 2010, **51**, 1341-1354.
54. C. Ma, M. Zhang and M. Rong, *J. Appl. Polym. Sci.*, 2007, **103**, 1578-1584.
55. S. Asai, K. Sakata, M. Sumita and K. Miyasaka, *Polym. J.*, 1992, **24**, 415-420.
56. D. Banerjee and K. S. Schweizer, *J. Polym. Sci., Part B: Polym. Phys.*, 2015. (DOI: 10.1002/polb.23752)
57. Y. Feng, N. Ning, Q. Zhao, J. Liu, L. Zhang, M. Tian and J. Mi, *Soft matter*, 2014, **10**, 8236-8244.
58. A. R. Hopkins and J. R. Reynolds, *Macromolecules*, 2000, **33**, 5221-5226.
59. M. Á. Corres, A. Mugica, P. M. Carrasco and M. M. Cortázar, *Polymer*, 2006, **47**, 6759-6764.
60. S. C. Tjong, G. Liang and S. Bao, *Polym. Eng. Sci.*, 2008, **48**, 177.
61. W. Zhang, A. A. Dehghani-Sanij and R. S. Blackburn, *J .Mater. Sci.*, 2007, **42**, 3408-3418.
62. S. Hölzer, M. Menzel, Q. Zia, U. S. Schubert, M. Beiner and R. Weidisch, *Polymer*, 2013, **54**, 5207-5213.
63. M. G. Broadhurst, *J. Res. Natl. Bur. Stand. A*, 1962, **66**, 241-249.
64. B. Wunderlich and G. Czornyj, *Macromolecules*, 1977, **10**, 906-913.
65. G. Höhne, *Polymer*, 2002, **43**, 4689-4698.
66. M. Kakudo and R. Ullman, *J. Polym. Sci.*, 1960, **45**, 91-104.
67. R. Androsch, J. Blackwell, S. Chvalun and B. Wunderlich, *Macromolecules*, 1999, **32**, 3735-3740.
68. L. H. Sperling, *Introduction to physical polymer science*, John Wiley & Sons, 2005.
69. J. Minick, A. Moet, A. Hiltner, E. Baer and S. Chum, *J. Appl. Polym. Sci.*, 1995, **58**, 1371-1384.
70. S. Bensason, E. Stepanov, S. Chum, A. Hiltner and E. Baer, *Macromolecules*, 1997, **30**, 2436-2444.
71. H. Wang, S. Chum, A. Hiltner and E. Baer, *J. Appl. Polym. Sci.*, 2009, **113**, 3236-3244.

Table of contents entry

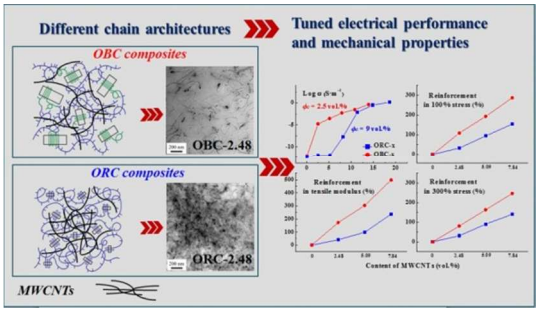

A new guidance for the development of conductive elastomers with improved comprehensive performance by considering chain architecture is provided.